Enhancing Spectrally Selective Response of W/WAlN/WAlON/Al_2O_3 –Based Nanostructured Multilayer Absorber Coating through Graded Optical Constants

Atasi Dan [a], Arup Biswas [b], Piyali Sarkar [b], Sanjay Kashyap [c], Kamanio Chattopadhyay [c, d], Harish C. Barshilia [e, *], Bikramjit Basu [a, d, *]

[a] Materials Research Centre, Indian Institute of Science, Bangalore 560 012, India

[b] Spectroscopy Division, Bhabha Atomic Research Centre, Mumbai 400085, India

[c] Materials Engineering, Indian Institute of Science, Bangalore 560 012, India

[d] Interdisciplinary Centre for Energy Research, Indian Institute of Science, Bangalore 560 012, India

[e] Nanomaterials Research Laboratory, Surface Engineering Division, CSIR-National Aerospace Laboratories, HAL Airport Road, Kodihalli, Bangalore 560 017, India

Abstract

In the field of concentrating solar power (CSP) technologies, multilayer absorber coatings are widely being investigated. The spectral properties of selective coatings can be tailored by carefully adjusting the composition and thickness of each layer. Based on the extensive analysis using the transmission electron microscopy (TEM), phase modulated spectroscopic ellipsometry along with computational analysis, we demonstrate how we can engineer the optical constants (refractive index and extinction coefficient) of individual layer to successfully achieve the spectrally selective properties in W/WAlN/WAlON/Al_2O_3 –based multilayer absorber coating. This coating exhibits a high absorptance of 0.958 and a low emittance of 0.08. The spectroscopic ellipsometry study confirmed the variation in metallic and optical properties of single layer of WAlN, WAlON and Al_2O_3 films, deposited on stainless steel substrates. This study also revealed the presence of intermediate layers of 26%

WAlN - 74% WAlON at WAlN/WAlON interface and 60% WAlON - 40% Al_2O_3 at WAlON/Al_2O_3 interface. The Tauc - Lorentz dispersion model was very effective to interpret the ellipsometry data of single layers of WAlN and Al_2O_3, while Cauchy absorbent model was useful for WAlON coating. Bruggeman effective medium approximation was used to describe the optical functions of intermediate layers. Investigation on optical constants reveals that the refractive index and extinction coefficient of each layer decrease from substrate to surface. The computational predictions of the reflectance properties corroborate well with the experimental results. In summary, the careful engineering on the optical properties of W/WAlN/WAlON/Al_2O_3 structure enables it to be an exceptional spectrally selective absorber coating.

Keywords: Spectrally selective coating, Transmission electron microscopy, Ellipsometry, optical constants

* **Corresponding Authors:**

Email: harish@nal.res.in (Harish C. Barshilia)

bikram@mrc.iisc.ernet (Bikramjit Basu)

1. Introduction

It is well known that the interaction of electromagnetic radiation with a material is described in terms of optical constants (refractive index, extinction coefficient, permittivity, etc.) [1]. The optical constants of solar selective coatings have attracted considerable interest since they constitute a major role in the spectrally selective absorber for photothermal conversion in concentrated solar power systems [2, 3]. The photo thermal conversion of solar energy requires an efficient solar selective absorber coating, which has a maximum absorptance ($\alpha \geq 0.95$) in solar irradiation region (0.25 - 2.5 μm) and minimum emittance ($\varepsilon \leq$ 0.05) in IR region (2.5 - 25 μm) [4, 5]. In order to understand the physical mechanism of

solar selectivity in an absorber coating, an extensive knowledge of optical constants over a wide range of wavelength is essentially important. The optical constants do not only help to determine the efficiency of a solar thermal systems, but also serve the role as an additional tool for optimization in designing the absorber coating in future. In recent years, several investigations are reported to understand the effect of optical constants. The role of refractive index and extinction co-efficient on reflectance properties of each layer have been established. Ellipsometry is widely used to determine the refractive index and extinction co-efficient of each layer [6, 7]. For example, Selvakumar et al. [8] performed the ellipsometric characterization on HfO_x/Mo/HfO_2 –based solar selective coating and found the metallic character of Mo layer, while dielectric behaviour has been observed in HfO_x and HfO_2 layers. An investigation using spectroscopic ellipsometry by Juang et al. [9] demonstrated that the property of stainless steel can change from metal to dielectric, if deposited in a nitrogen environment. Soum-Glaude et al. [10] analysed the spectral performance of SiC(N)H coating with the help of ellipsometric measurements while Subasri et al. [11] confirmed the fabrication of graded index structure of Ag-TiO_2/TiO_2/SiO_2 absorber coating.

In order to advance the optical engineering of the thin film and to comprehend the light trapping phenomenon, different simulation approaches are adopted and applied for single and multilayer coatings. Irrespective of the approach and coating structures, most of the simulation procedures require the known optical constants as input. In addition, a number of other parameters such as the number of layers, their order and thicknesses are also required. This aspect has been reported to a larger extent. Farooq et al. [12] have simulated the optical properties of a multilayer V:Al_2O_3 coating with a high absorptance of 0.98 and a low emittance of less than 0.07 using a computer model. They also validated the computational findings with experimental results. Modelling of two multilayer stacks (Mo, TiO_2, MgF_2 and W, TiO_2, MgF_2) have been performed by Sergeant et al. [13]. They predicted

high solar absorptance (> 94%), while thermal emittance was low (< 7%) at 720 K. Nejati et al. [14] have theoretically investigated the optical properties of absorber coatings by changing the number of cermet layers with different ceramic and metallic components.

In our previous work [15, 16], we have reported the spectrally selective properties (α = 0.958, ε = 0.08) of W/WAlN/WAlON/Al_2O_3 –based solar absorber coating, which was deposited on stainless steel substrate by reactive DC and RF magnetron sputtering. The coating also possessed a high angular absorptance over a wide range of incidence angles from 18° - 58° [17].

In the present study, we have unravelled the mechanism of the superior selectivity of W/WAlN/WAlON/Al_2O_3 -based absorber coating. We have examined and analysed each layer of the coating systematically using transmission electron microscopy (TEM). The optical constants of all the layers were evaluated using spectroscopic ellipsometry data. The reflectance spectra of the coatings were simulated with commercially available SCOUT software by modelling the multilayer absorber stack. The obtained results and subsequent analysis enable appropriate explanation for the origin of spectrally selective properties of W/WAlN/WAlON/Al_2O_3 coating.

2. Experimental

W/WAlN/WAlON/Al_2O_3 multilayer coating has been deposited on stainless steel (35 mm X 35 mm X 2 mm) and Si substrates by reactive DC and RF magnetron sputtering. Mechanically polished and chemically cleaned substrates were kept in the sputtering chamber which was pumped to a base pressure of 8.5 X 10^{-6} mbar. High purity (> 99.9%) W, Al and Al_2O_3 targets were used for deposition. Reactive DC sputtering of W and Al targets was carried out in order to deposit WAlN and WAlON layers in Ar + N_2 and Ar + N_2 + O_2, respectively. The Al_2O_3 layer was deposited by RF sputtering in Ar + O_2 environment. Proper

optimization of target power, deposition time and gas flow rate resulted in desired selective coating with maximum solar absorptance and minimum thermal emittance. Gas flow was controlled by electronic mass flow controllers and the substrates were continuously rotated during deposition. The deposition parameters have been demonstrated in detail elsewhere [15].

Detailed microstructural and chemical characterization of all the layers were carried out using FEI make TITAN G^2 60-300kV TEM/STEM. For this study, we prepared the cross-sectional TEM samples using thinning of samples by dimpling, followed by ion milling (Gatan make PIPS). High-resolution transmission electron microscopy (HR-TEM), and selected area electron diffraction (SAED) studies were also performed to acquire further information. The thickness of the single layer WAlN, WAlON and Al_2O_3, deposited for longer duration on Si substrates were measured by FESEM. The surface roughness of films fabricated on stainless steels were examined using AFM (Bruker).

The ellipsometric data were collected using a spectroscopic phase modulated ellipsometer (model UVISEL™ 460, ISA JOBIN-YVON SPEX) in the wavelength range of 300 – 800 nm at an incidence angle of 70°. The data analysis was carried out using DeltaPsi2 Software. A Perkin-Elmer Lambda 950 spectrophotometer equipped with an integrating sphere of diameter 150 mm were used in the wavelength interval 0.3 – 2.5 μm to measure diffuse reflectance of the coatings. The experimental reflectance spectra were fitted with the SCOUT software. In order to facilitate the simulation procedure, we used optical constants obtained from ellipsometry study and angle of incidence as input.

3. Results

3.1. Microstructural Properties

First, we shall present the microstructural details of the investigated multilayer coating. TEM investigation of the cross-sectional absorber reveals the thickness of individual layer of W, WAlN, WAlON, and Al_2O_3 to be ~125 nm, ~40 nm, ~40 nm and ~62 nm, respectively. A ~ 4 nm thin silicon oxide layer could also be observed on Si substrate. Dark field TEM micrograph of Fig. 1 (a), acquired using STEM dark-field detector, clearly shows the growth of all the four layers. The compositions of each of the four layers were determined by carrying out line scans across the layers. The concentration profiles of each element are shown in Fig. 1 (b) and the corresponding traces of the beam is shown by the red line in the TEM micrograph of Fig. 1 (a). Each layer is clearly distinguishable in terms of variation in elemental concentration, as marked in Fig. 1 (b). Selected area electron diffraction (SAED) pattern acquired from the substrate (Fig. 1 (c)) can be indexed in terms of [101] zone axis of Si. Fig. 1 (d) shows the dark-field TEM image along with SAED pattern in the inset. The SAED can be indexed in terms of [001] zone axis of bcc W. The dark-field image is acquired using (020) reflection of bcc W. The SAED pattern acquired from the grain is shown by the arrow. This evidence confirms the crystalline nature of W layer. At few places in the dark-field image, a number of fine nanocrystals are also illuminated in WAlN and Al_2O_3 layers. Such observations indicate the nanocrystalline nature of these layers. Diffuse spotty ring in the diffraction pattern and the dark-field image in Fig. 1 (e) also support such observations. Most of the spotty rings can be indexed as the reflections of hexagonal α-Al_2O_3. The dark-field image corresponds to (202) reflection of α-Al_2O_3. The uniform contrast of the WAlON layer suggests the possible amorphous nature of this layer. To further support the above results, we have carried out high-resolution transmission electron microscopy (HRTEM) of interfaces (details are in supplementary information, Fig. S1).

3.2. Spectroscopic Ellipsometry Analysis

3.2.1 Optical Functions of Single Layer Coatings

An analysis of selective properties of a multilayer film requires a knowledge on the optical properties of individual layer. In order to obtain the optical properties of individual layer, single layer of WAlN, WAlON and Al_2O_3 were fabricated independently on stainless steel and Si substrates for longer duration. Before starting the ellipsometric study, it was necessary to acquire information about the thickness of each single layer coating. Hence, the individual coating on Si substrate was investigated using FESEM for the cross-sectional thickness measurements. The thicknesses of the coatings are found to be ~ 433, 716 and 300 nm for WAlN, WAlON and Al_2O_3 films, respectively (Supplementary information; Fig. S2.).

In spectroscopic ellipsometry, the main principle is to measure the changes in the state of the polarization of a monochromatic beam upon reflection at an optical boundary. The changes are expressed as Ψ and Δ of each layer, which correspond to changes in amplitude ratio and phase of s- and p- polarised light, respectively. Ψ and Δ are related by the complex reflection ratio (ρ), i.e., the ratio of the Fresnel reflection coefficients for *s*- and *p*-polarized light [18]:

$$\rho = \frac{r_p}{r_s} = \tan(\Psi)\exp(i\Delta) = \frac{\frac{E_{rp}}{E_{ip}}}{\frac{E_{rs}}{E_{is}}} \quad (1)$$

where E_{rp} and E_{rs} are the reflected electric fields for *s*- and *p*- polarized light, respectively, and E_{ip} and E_{is} are the respective incident electric fields.

The optical constants can be determined by considering a proposed physical model corresponding to each sample which can be generated based on appropriate generalised oscillator for the optical dispersion. Eventually curve fitting of the obtained data from the proposed model can be carried out with the experimental Ψ and Δ data, acquired from ellipsometry. The goal is to minimize the mean square function using a regression algorithm for the ellipsometry equation [19]:

$$\chi = \left\{ \frac{1}{2N-M} \sum_{i=1}^{N} \left[\left(\frac{\Psi_i^{mod} - \Psi_i^{expt}}{\sigma_{\Psi,i}^{expt}} \right)^2 + \left(\frac{\Delta_i^{mod} - \Delta_i^{expt}}{\sigma_{\Delta,i}^{expt}} \right)^2 \right] \right\}^{1/2} \quad (2)$$

where N is the number of measured Ψ and Δ pairs, M is the total number of variable parameters, and σ is the standard deviations. The superscript 'mod' means the theoretical calculations and the 'expt' means the experimental data.

The fitting of the experimentally measured ellipsometric parameter (Ψ and Δ) with theoretically generated parameters were performed using the following approaches:

a) A single layer homogeneous model of thin film was constructed with a realistic dispersion model of refractive index (*n*) and extinction coefficient (*k*).

b) The optical properties (*n* and *k*) of substrate were taken from separate ellipsometric measurement of bare substrate.

c) The dispersion modelling of the optical properties of WAlON layers was performed using Cauchy absorbent dispersion relation due to amorphous nature of the sample. The Cauchy absorbent dispersion relation can be expressed as,

$$n(\lambda) = A + \frac{B}{\lambda^2} + \frac{C}{\lambda^4} \quad (3)$$

$$k(\lambda) = D + \frac{E}{\lambda^2} + \frac{F}{\lambda^4} \quad (4)$$

where λ is the wavelength, A, B, C, D, E and F are the fit parameters. A represents the long wavelength asymptotic refractive index value. B and C influence the slope and amplitude of the refractive index curve. B dominates the curvature for the medium wavelength, while C is responsible for the spectrum at shorter wavelengths. The characteristics of D, E and F are similar to A, B and C respectively.

(d) We preferred using a Tauc–Lorentz (TL) oscillator model for WAlN and Al_2O_3 coating as some nanograins are visible in these layers (see S1 (d)). TL model is very effective in characterization of nanocrystalline and amorphous materials [20]. It is relevant to mention that the complex dielectric function for a material can often be expressed using such simple oscillator model. This model provides the expression for ε_2, the imaginary part of the dielectric function. The model can be obtained by multiplying the Tauc expression for ε_2 near the band edge by the imaginary part of the complex dielectric function of a single Lorentz oscillator [21]:

$$\left.\begin{aligned} \varepsilon_2 &= \frac{AE_O\Gamma(E-E_g)^2}{\left[\left(E-E_g\right)^2+\Gamma^2E^2\right]^2}\frac{1}{E}\,;\ \mathrm{E} > \mathrm{E_g} \\ \varepsilon_2 &= 0\,;\qquad\qquad \mathrm{E} < \mathrm{E_g} \end{aligned}\right\} \tag{5}$$

where E_o is the peak transition energy, E_g is the optical band gap energy, Γ is the broadening parameter, and A is the optical transition matrix elements. The real part of the dielectric function ε_1 is given by Kramers-Krönig transformation (KKT)

$$\varepsilon_1 = \varepsilon_{\alpha,UV} + \frac{2}{\pi}P\int_{E_b}^{\infty}\frac{\xi\varepsilon_2(\xi)}{\xi^2-E^2}d\xi \tag{6}$$

where $\varepsilon_{\alpha,UV}$ is high frequency dielectric constant and P is denoting the principal values of the integrals. This integral could be solved in the closed form, which is shown elsewhere [21, 22].

These proposed physical models have been curve fitted with experimentally measured Ψ and Δ data of WAlN, WAlON and Al_2O_3 samples through $\boldsymbol{\chi}^2$ minimisation (metric of good fitting) process. The maximum number of iteration allowed is 100 and the criteria for convergence used is $\delta\boldsymbol{\chi}^2 = 0.000001$. Clearly, the fitted Ψ and Δ, marked by solid lines are in good agreement to the measured data, represented by open symbols in Figs. 2 (a - c). The respective single layer structures used to perform the modelling have also been presented

along with $\Psi - \Delta$ spectrum. However, the oscillations in the full wavelength range of 300 – 800 nm in Figs. 2 (b) and 2 (c) indicate interference phenomenon representing the semi-transparent/transparent behaviour of WAlON and Al_2O_3. In contrast, the absence of such oscillation in Fig. 2 (a) is indicative of strongly absorbing property of WAlN. Such behaviour can also be predicted from the reflectance spectra of each single layer coating in the wavelength range of 300 - 2500 nm (see supplementary information, Fig. S3.). The optical constants, refractive index (n) and extinction coefficient (k) of the individual layer have also been extracted from the best fitting results of Cauchy absorbent dispersion relation and TL model and plotted as a function of wavelength in Figs. 3 (a) and 3 (b). It can be noted that the refractive index of WAlN increases with wavelength, which is a characteristic response of metallic film. In case of WAlON, the refractive index slowly decreases with wavelength and does not show much variation after 600 nm, which can be considered as an evidence of semiconducting nature of WAlON [23, 24]. Al_2O_3 has almost a constant refractive index throughout the wavelength range. The decrease of the k in WAlN and WAlON film depicts the existence of interband transition. The 'k' value of Al_2O_3 is zero as expected for a dielectric material (see Fig. 3 (b)) [25]. Such excellent optical behaviour makes Al_2O_3 a very good option for anti-reflection layer. The best fitting parameters for all the layers have been presented in Tables 1 and 2.

The optical absorption co-efficient defines how far can electromagnetic radiation of a particular wavelength can penetrate a material. This can be calculated in terms of wavelength and the optical extinction co-efficient by the following equation

$$\alpha = \frac{4\pi k}{\lambda} \tag{7}$$

Absorption coefficient of WAlN, shown in Fig. 4 (a) is appreciably higher than that of WAlON and Al_2O_3. Such observation indicates that WAlN absorbs photons very efficiently than other two films, which is also evident from the variation of penetration depth as a

function of wavelength in Fig. 4 (b). The penetration depth provides useful information on the thickness of the material involved in the interaction with light [26]. As seen in Fig. 4 (b), the penetration depth in WAlN film is almost zero, which physically signifies that the solar radiation is trapped in the film while for WAlON layer, the penetration depth increases drastically with wavelength. This indicates the solar radiation can penetrate the WAlON film intensely before getting absorbed. These results also suggest that WAlN is the main absorbing layer of the multilayer structure, while WAlON acts as semi-transparent layer.

The optical constants (n and k) are related to complex dielectric constant by the following expression, $\varepsilon = \varepsilon_1 + i\varepsilon_2$, where $\varepsilon = N^2$ and the complex refractive index, $N = n + ik$. Hence, $\varepsilon_1 = n^2 - k^2$and $\varepsilon_2 = 2nk$ [27]. Figs. 4 (c) and 4 (d) represent the real and imaginary part of ε as a function of incident photon energy. The imaginary part of the dielectric constant is directly related to the conductivity, which can be observed from the equation below.

$$\varepsilon = \varepsilon_1 + i\varepsilon_2 = \varepsilon_1 + i\frac{\sigma\omega}{\varepsilon_o} \tag{8}$$

Therefore, more the value of ε_2, more conducting the material will be. Hence, the large ε_2 of WAlN in Fig. 4 (d) suggests the conducting i.e. metallic property of that layer. The imaginary part of dielectric function is also associated with the dissipation and thus it is responsible for the absorption. It is well known that the higher the imaginary part of the complex dielectric constant, better the wave absorption effect. Therefore, the high value of ε_2 is responsible for the maximum absorption of solar energy in WAlN. The lower ε_2 values for WAlON and Al_2O_3 film represent the transmitting behaviour of these layers. All these findings from dielectric constant data validate the observations found in the previous observations related to optical constants, absorption coefficients and penetration depths of all the layers.

3.2.2. Optical Functions of Multilayer Coatings

The optical design of multilayer coatings was performed using the optical constants of single layers, evaluated using Cauchy absorbent dispersion model and TL model. It is important to mention here that W layer possess pure metallic character with a high refractive index (n = 3.83), which has been well reported in literature [28, 29]. Moreover, W layer does not have any role in increasing the absorption of solar radiation in W/WAlN/WAlON/Al_2O_3 stack. Therefore, initially, we considered the basic layer-by-layer structure of WAlN/WAlON and WAlN/WAlON/Al_2O_3 and made an attempt to fit the experimental ellipsometric data of these samples deposited on SS substrate. However, we were unable to fit the experimental data with the theoretical predicted spectra. This may be due to the fact that the layer-by-layer stack is oversimplified. Hence, simple Cauchy absorbent and TL dispersion model cannot solely explain the optical response of such complicated structure. When we are moving from single layer to multilayer stack, we must take into account the collective optical behaviour of neighbouring layer and their effect on each other. Therefore, we consider a multilayer model, where the presence of intermixed layers was assumed in the middle of two layers. The intermediate layer in between WAlN and WAlON, WAlN-WAlON has been considered as a mixture of WAlN and WAlON phases. On the other hand, WAlON-Al_2O_3 is an intermixing layer in between WAlON and Al_2O_3 films. Due to complexity of the interfacial layer properties, researchers have often used Bruggeman effective-medium approximation (EMA)[30] model to obtain the optical properties of a two mixed material such as,

$$f_A \frac{\varepsilon_A - \varepsilon^{BR}}{\varepsilon_A + 2\varepsilon^{BR}} + (1 - f_A) \frac{\varepsilon_B - \varepsilon^{BR}}{\varepsilon_B + 2\varepsilon^{BR}} = 0 \qquad (9)$$

where ε^{BR} is the average dielectric function of the composite in Bruggeman approximations, ε_A and ε_B indicate the dielectric function phase A and phase B, respectively. The filling factor f_A is the volume fraction occupied by phase A.

However, EMA model is very sensitive to the surface morphologies. The surface roughness can significantly influence the fitting using EMA model. The surface roughnesses of layer by layer coatings are notably small (~ 1 - 2 nm) (Supplementary information, Fig. S4.). Therefore, the effect of the surface roughness has been neglected.

The variation of Ψ and Δ for WAlN/WAlN-WAlON/WAlON and WAlN/WAlN-WAlON/WAlON/WAlON-Al_2O_3/Al_2O_3 coatings on SS substrates in the wavelength range of 300 - 800 nm have been shown in Figs. 5 (a) and 5 (b). The experimental and analytically predicted data are in well agreement with each other, which gives more confidence to the model used (see insets of Figs. 5 (a) and 5 (b)). The best fit results have been chosen by optimising simultaneously the composition of intermediate layers. The intermixed layer in between WAlN and WAlON contains 26% WAlN and 74% WAlON, while the layer in between WAlON and Al_2O_3 is a mixture of 40% WAlON and 60% Al_2O_3. The EMA model has been utilized to generate the optical constants of the intermixed layers by weighting the optical constants of their components. We have also presented the wavelength dependence of n and k in Figs. 6 (a) and 6 (b). Interestingly, the optical constants (n and k) systematically decrease from WAlN (bottom layer) to Al_2O_3 (top layer). The optical constants of all the layers at 550 nm have been summarized in Table 3.

3.3. Optical Simulation

We have performed computational studies based on optical constants of the individual layer to predict reflectance properties in 300 – 2500 nm wavelength range. The simulated spectra using SCOUT software was fitted with the measured reflectance spectra by adjusting the optical constants of the individual layer. Optical constants of all the layers including the substrate, obtained from spectroscopic ellipsometry measurement have been introduced during simulation to calculate the reflectance. Figs. 7 (a) and 7 (b) show that the simulated and the experimental spectra do not agree well with each other as we did not consider the

presence of intermediate layers (WAlN - WAlON and WAlON - Al_2O_3). However, Figs. 7 (c - e) illustrate best fitted simulated and reflectance spectra, where the optical constants of all the five layers (WAlN, WAlN-WAlON, WAlON, WAlON-Al_2O_3 and Al_2O_3) acquired from ellipsometry study, were used to conduct computational analysis for the multilayer stack with two intermediate layers. Hence, the formation of the intermediate layer is also validated by the computational study. It can also be observed that in case of the coatings without the intermixed layers (Figs. 7 (a) and 7 (b)), the reflectance minima of all the spectra appear in the lower wavelength side, whereas the reflectance spectra of the thin films (Figs. 7 (c - e)) simulated by introducing the middle layers indicate a shift in the reflectance minima towards higher wavelength. It causes the reduction of the reflectance in the solar spectrum, thus increasing the absorptance of the coating. This study also confirms the accuracy of the optical constants, which were used to simulate the reflectance spectra. Therefore, it should be mentioned that the simulation in the present study can be considered to be an innovative reverse engineering procedure, which is extremely effective to verify the optical constants of the candidate layers, originated from ellipsometry.

4. Discussion

The most significance outcome of the present work has been to establish the rationale behind the remarkable spectrally selective properties of W/WAlN/WAlON/Al_2O_3 with the help of spectroscopic ellipsometry measurements and computational analysis. In the following, we shall describe the correlation between architecture of the coating and optical constants as well as underlying physical mechanism of solar energy absorption.

4.1. Correlation between Optical Properties of Tandem Absorber and Multilayer Architecture

4.1.1. Gradation in Refractive Index

The investigation on the single and multilayer coating has demonstrated specific dependence of optical constants (n and k) of all the layers on the wavelength. According to the previous study of our group, WAlN/WAlON/Al_2O_3 has a very high absorptance of 0.958 in the solar spectrum. As the optical constants play an important role to design an efficient spectrally selective coating, it can be predicted that the appropriate stacking of these layers have offered such remarkable solar absorptance in the solar wavelength range. The successful fabrication of WAlN/WAlON/Al_2O_3 coating is directly related to the optical constants, particularly refractive index of each layer. A small difference in the refractive index may lead to a drastic change in the selective performance of the coating. Our study confirms that WAlN has a strongly absorbing property, while Al_2O_3 layer is transparent due to its dielectric nature. It is also evident from Fig. 6 (a) that WAlN/WAlON/Al_2O_3 is a graded film, where the refractive index of the individual layer is different from those of neighbouring layer. Also, the refractive indices of the coating decrease form substrate to surface.

The most exciting finding of this work is the existence of the intermediate layers. There is no sharp boundary among WAlN, WAlON and Al_2O_3 layers. These layers are connected by two intermediate layers of 26% WAlN - 74% WAlON and 60% WAlON - 40% Al_2O_3. Fig. 6 (a) indicates that the refactive index of 26% WAlN - 74% WAlON layer lies in between the refractive indices of WAlN and WAlON, while 60% WAlON - 40% Al_2O_3 layer also shows intermediate value of refractive index following the analogy of the previous junction layer. The appropriate modelling to capture the reflectance properties of the multilayer stack was the major challenge of this work. This was accomplished by introducing the interfacial layers and optimizing appropriate volume fraction of the components in the interfacial layers. In particular, the analysis using EMA model enabled us to understand that the formation of these two additional intermediate layers makes the film highly graded. This kind of variation in refractive index makes the three-layer stack effectively five layer stack. It

is noteworthy to mention that the high absorptance and the gradation in refractive indices are highly correlated with each other. Therefore, it can be interpreted that the approach of decreasing refractive index from the base layer to surface of a multilayer coating is an unavoidable restriction for a solar selective absorber coating. The gradation of refractive index has been introduced by varying the gas flow of N_2 and O_2 as the refractive index of any layer is strongly dependent of the composition. The integration of N and O atoms in W and Al matrix changes the electronic configuration, chemical states and film properties. Bartzsch et al.[31] demonstrated the nonlinear dependency of the refractive index on the oxygen content. They reported a decrease in refractive index with an increase in oxygen component in $Si_xO_yN_z$ film. Borges et al.[32] were also able to tailor the optical properties of AlN_xO_y film by changing N_2 + O_2 reactive gas mixture. Therefore, it is expected that the successive deposition of all the layers in different reactive gas environment resulted in the formation of an optically graded film. On the other hand, the refractive index of a coating is directly related to the metallic property of the coating. The refractive index of the coating increases with an increase in metallic property. This can also be supported from the extinction coefficient (k) of each layer. One can notice in Fig. 6 (b) that WAlN has the maximum value of k and for Al_2O_3, k = 0. It is well known that materials with lower value of k are dielectric, while those with higher value of k shows metallic property.

4.1.2. Compositional Variation

The decrease of the metallic property can be explained in the following way. W layer on stainless steel substrate is a pure metal and a source of free electrons. It is relevant to state that W layer serves the role of an infrared reflector to reduce the thermal heat loss from the coating i.e. emittance of the coating. Therefore, W/WAlN/WAlON/Al_2O_3 coating has a very low thermal emittance of 0.08. It also acts as a diffusion barrier to protect the film from degradation at high temperature. However, during deposition of WAlN layer, nitrogen gas is

impinged for reactive sputtering. In view of the microstructural properties, the W atoms can accommodate nitrogen atoms of smaller size with a distortion in the lattice, which leads to nanocrystalline nature of the film. Due to electronegative nature, N atoms acquire electrons at the expense of W and Al atoms and it acts as an attractive pole of free electrons supplied by W and Al. As a result, the conductivity of WAlN layer decreases to some extent compared to pure W metallic layer on stainless steel substrate. It has been observed by Soto et al. [33] that in low pressure of nitrogen, a component of WAlN film, WN_x exhibits metallic property. In a separate study [34], it has also been reported that WN_x has the lowest electrical resistivity among other transition metal nitrides. Even though the formation of semiconducting AlN takes place during sputtering, the metallic character is predominant due to the presence of WN_x as well as metallic Al in WAlN layer. Moreover, the higher value of complex dielectric constant of WAlN is correlated to the increased metallic property (see Fig. 4 (d)). During the fabrication of WAlON layer, the gas mixture of N_2 and O_2 is fed into the sputtering chamber. For the combined concentration of N and O atoms, it becomes impossible for these atoms to fit into W or Al atoms and the layer becomes completely amorphous. It is important to mention that the oxynitrides in this layer, WO_xN_y or AlO_xN_y are very attractive systems because optical properties of the constituent materials (Al, W, WO_x, Al_2O_3, WN_x, AlN, etc) can be tuned to achieve the required performance. A few studies [35, 36] have been focused on the optical properties of transition metal oxynitrides, particularly WO_xN_y compared to that of transition metal oxides or nitrides. It is worthwhile to state that W exhibits a stronger affinity to oxygen than nitrogen. Also, from the thermodynamic considerations, the formation of tungsten oxide is strongly favoured over the formation of tungsten nitride or NO, because the heat of formation for WO_3 and WO_2 is -842.9 kJ/mol [37] and -589.7 kJ/mol [38], respectively. Such values are much lower than corrosponding values for W_2N (-22 kJ/mol) [39], WN (-15 kJ/mol) [40], and NO (-91.3 kJ/mol) [41]. Therefore, it is expected that a large

portion of WAlON layer will be occupied by WO_3 and WO_2 phases. Moreover, Gillet et al. [42] suggested that the conductivity of WO_3 is related to non-stoichiometry, which originates from oxygen vacancies. In a separate study [43], it has been reported that amorphous WO_3 thin film has a band gap of 3.4 eV, while heat treated crystalline film possess a smaller band gap of 2.6 eV. Li et al. [44] also demonstrated that WO_3, a wide band n-type semiconductor with a conductivity of 3.5×10^{-11} S/cm, acts as insulator (1.6×10^{-8} S/cm) before annealing due to amorphous nature. As WO_xN_y system is composed of WO_3, WO_2, WO_x, WN, etc. phases, AlO_xN_y system in WAlON layer similarly may consist of substoichiometric AlO_x and AlN_y as well as stoichiometric Al_2O_3 and AlN. The band gap and conductivity of these materials can also be associated with the difference in ionicity between metal-O and metal-N bonds. As both these bonds present simultaneously in WAlON layer, these lead to the localisation of most of the free electrons in W and Al. Considering all these aspects, it can be commented that WAlON has a lower metallic property than WAlN. On the surface, the anti-reflecting layer is purely non-conducting as it contains Al_2O_3, a highly insulating material (E_g ~ 3.64 eV) consisted of mixed ionic and covalent bonding and a large band gap energy [45]. Hence, the descending order of metallic component from substrate to surface has been elucidated intensely.

4.2. Solar Energy Absorption Mechanism in Multilayer Stack

Now, we will try to explain the possible absorption mechanism, which is responsible for such an outstanding spectral selectivity of W/WAlN/WAlON/Al_2O_3 coating. An incident electromagnetic wave, while interacting with a material undergoes reflection, absorption and transmission. It is well known that it is difficult to achieve the highest spectral selectivity by a single layer due to huge amount of surface reflection. When light travels through the interface between two media with different refractive index (n_1 and n_2), the reflected light intensity at normal incidence can be expressed as,

$$R = \left[\frac{n_1 - n_2}{n_1 + n_2}\right]^2 \quad (10)$$

The above equation predicts that a strong reflection takes place, when the solar radiation tries to enter the main absorbing WAlN layer that typically have both a high real and imaginary part of the refractive index compared to air. In order to reduce the energy loss, it was essential to fabricate Al_2O_3 as an antireflection layer, which has a low refractive index. This simple concept of AR coating only works well for a limited range of wavelength and angle of incidence. A wide band and angularity independent reduction in the light reflection was achieved by depositing the semi-transparent WAlON layer in between WAlN and Al_2O_3 layers.

A coating with low metallic property and optical constants will allow the sunlight to transmit to the next layer. The light-matter interaction will be stronger in WAlN due to higher metallic properties. These claims can also be validated by the absorption co-efficient and penetration depth of WAlN layer (see Figs. 4 (a) and 4 (b)). Even though absorption is very high in WAlN, some portion of the sunlight will be reflected back to 26% WAlN – 74% WAlON layer from WAlN layer. According to ray optics, if two emerging reflected electromagnetic waves from WAlN and 26% WAlN – 74% WAlON layers are out of phase by 180°, they lead to an extinction of solar radiation due to destructive interference. Consequently, the absorptance increases drastically. The reflectance spectra of the samples in Figs. 7 (c - e) depict that the reflectance is effectively reduced by adding each additional layer, which signifies the enhancement in solar absorptance. The presence of two interference minima at 360 and 1293 nm can be observed in the reflectance spectrum of SS/W/WAlN/WAlON, while the appearance of a wider minimum occupying wavelength of 870 – 1345 nm along with a sharp minimum at 356 nm can be distinctly noticed in the reflectance spectrum of SS/W/WAlN/WAlON/Al_2O_3. Therefore, the occurrence of

destructive interference in the presently studied coating can be believed to be of great significance to boost the solar absorptance in solar spectrum.

Another interesting approach to capture the solar radiation is through total internal reflection (TIR), caused by the refractive index contrast between the neighbouring layers. The solar rays scatter in different direction during interaction with the nanocrystallines in WAlN layer. If the rays fail to fall within the escape cone, described by the critical angle[46], $\theta_c = arcSin\left(\frac{n_{26\%\,WAlN-74\%\,WAlON}}{n_{WAlN}}\right)$, the rays will be totally internally reflected backed to WAlN layer. The reflection of the rays for other layers is analogous to WAlN layer. The multiple reflections of the rays increase the possibility of light-matter interaction and the absorptance increases remarkably. Moreover, nanocomposite structure of WAlN layer, embedded in amorphous matrix is very effective for intrinsic absorption of solar radiation. The high value of extinction coefficient of WAlN accounts for the strong absorption in solar wavelength range.

In summary, the specific design of W/WAlN/WAlON/Al_2O_3 with a gradient in the refractive index (n) and extinction coefficient (k) gradually from substrate to surface enabled the coating to have outstanding solar radiation absorption ability (α = 0.958) with a minimum heat loss into the surrounding (ε = 0.08). Three optical phenomena; i.e., interference mechanism, total internal reflection and intrinsic absorption have major contributions to boost solar absorptance significantly.

It is also important to mention that the thermal, structural and chemical stability are the most essential criteria for a coating to be a potential high temperature spectrally selective surface. In our recent study, we have reported that W/WAlN/WAlON/Al_2O_3 coating was stable at 350 and 500 °C in air for 500 and 150 hrs, respectively without showing any significant change in the selective performance [17, 47]. The structural and chemical characterizations of the as-deposited and annealed coatings also suggested the outstanding

stability of the different components present in the coating at high temperature. Hence, it can be stated that the presently studied coating undoubtedly have the potential to emerge as a spectrally selective solar absorber coating for solar thermal power systems.

5. Conclusions

In the present work, the microstructural study, phase modulated ellipsometric analysis together with computational analysis using SCOUT software have revealed the reasons behind the outstanding selective properties of W/WAlN/WAlON/Al_2O_3 –based solar selective absorber coating fabricated using magnetron sputtering. The key findings are as follows:

a) TEM analysis confirms the crystalline nature of W layer. The existence of very fine nanocrystals in WAlN and Al_2O_3 layers was recorded together with amorphous nature of WAlON layer.

b) Based on the critical analysis of the phase modulated ellipsometry data using Cauchy absorbent dispersion model, Tauc-Lorentz and Bruggeman effective medium approximation model, the gradation in optical constants (n and k) across the tandem architecture was established. During the analysis of the spectroscopic ellipsometry data, it has been perceived that the presence of two additional layers of 26% WAlN - 74% WAlON at WAlN/WAlON interface and 60% WAlON - 40% Al_2O_3 at WAlON/Al2O3 interface can allow one to effectively establish good corroboration between experimentally measured and model based predicted data. Bruggeman effective medium approximation works very well in parameterizing the refractive index and extinction coefficient of the intermediate layers.

c) The computational analysis using the extracted optical constants from ellipsometry study establishes a good corelation between simulated and measured reflectance spectra of the multilayer coating.

Overall, the combined study of fine scale microstructural analysis, ellipsometric measurements and the simulation work provide us effective guidelines to understand the solar selective properties of W/WAlN/WAlON/Al_2O_3 absorber coatings.

Acknowledgments:

The authors thank Mr. Srinivas, Mr. Praveen Kumar and Mr. Siju for UV-Vis-NIR, AFM and SEM measurements. Research at CSIR-NAL is partially supported by Department of Science and Technology, New Delhi (U-1-144). This paper is based upon work supported in part under the US-India Partnership to Advance Clean Energy-Research (PACE-R) for the Solar Energy Research Institute for India and the United States (SERIIUS), funded jointly by the U.S. Department of Energy (Office of Science, Office of Basic Energy Sciences, and Energy Efficiency and Renewable Energy, Solar Energy Technology Program, under Subcontract DE-AC36-08GO28308 to the National Renewable Energy Laboratory, Golden, Colorado) and the Government of India, through the Department of Science and Technology under Subcontract IUSSTF/JCERDC-SERIIUS/2012 dated 22nd Nov. 2012. AD acknowledges DST for providing INSPIRE scholarship.

References

[1] E.D. Palik, Handbook of optical constants of solids, Academic press, 1998.
[2] D. Barlev, R. Vidu, P. Stroeve, Innovation in concentrated solar power, Solar energy materials and solar cells, 95 (2011) 2703-2725.
[3] H.L. Zhang, J. Baeyens, J. Degrève, G. Cacères, Concentrated solar power plants: Review and design methodology, Renewable and Sustainable Energy Reviews, 22 (2013) 466-481.
[4] N. Selvakumar, H.C. Barshilia, Review of physical vapor deposited (PVD) spectrally selective coatings for mid-and high-temperature solar thermal applications, Solar energy materials and solar cells, 98 (2012) 1-23.
[5] A. Dan, H.C. Barshilia, K. Chattopadhyay, B. Basu, Solar energy absorption mediated by surface plasma polaritons in spectrally selective dielectric-metal-dielectric coatings: A critical review, Renewable and Sustainable Energy Reviews, 79 (2017) 1050-1077.

[6] P. Löper, M. Stuckelberger, B. Niesen, J. Werner, M. Filipic, S.-J. Moon, J.-H. Yum, M. Topič, S. De Wolf, C. Ballif, Complex refractive index spectra of $CH_3NH_3PbI_3$ perovskite thin films determined by spectroscopic ellipsometry and spectrophotometry, The journal of physical chemistry letters, 6 (2014) 66-71.
[7] J.Q. Xi, M.F. Schubert, J.K. Kim, E.F. Schubert, M. Chen, S.-Y. Lin, W. Liu, J.A. Smart, Optical thin-film materials with low refractive index for broadband elimination of Fresnel reflection, Nature photonics, 1 (2007) 176-179.
[8] N. Selvakumar, H.C. Barshilia, K.S. Rajam, A. Biswas, Structure, optical properties and thermal stability of pulsed sputter deposited high temperature HfO_x/Mo/HfO_2 solar selective absorbers, Solar Energy Materials and Solar Cells, 94 (2010) 1412-1420.
[9] R.-C. Juang, Y.-C. Yeh, B.-H. Chang, W.-C. Chen, T.-W. Chung, Preparation of solar selective absorbing coatings by magnetron sputtering from a single stainless steel target, Thin Solid Films, 518 (2010) 5501-5504.
[10] A. Soum-Glaude, I. Bousquet, L. Thomas, G. Flamant, Optical modeling of multilayered coatings based on SiC(N)H materials for their potential use as high-temperature solar selective absorbers, Solar energy materials and solar cells, 117 (2013) 315-323.
[11] R. Subasri, K.R.C.S. Raju, D.S. Reddy, N.Y. Hebalkar, G. Padmanabham, Sol–gel derived solar selective coatings on SS 321 substrates for solar thermal applications, Thin Solid Films, 598 (2016) 46-53.
[12] M. Farooq, M.G. Hutchins, A novel design in composities of various materials for solar selective coatings, Solar energy materials and solar cells, 71 (2002) 523-535.
[13] N.P. Sergeant, O. Pincon, M. Agrawal, P. Peumans, Design of wide-angle solar-selective absorbers using aperiodic metal-dielectric stacks, Optics express, 17 (2009) 22800-22812.
[14] M.R. Nejati, V. Fathollahi, M.K. Asadi, Computer simulation of the optical properties of high-temperature cermet solar selective coatings, Solar Energy, 78 (2005) 235-241.
[15] A. Dan, J. Jyothi, K. Chattopadhyay, H.C. Barshilia, B. Basu, Spectrally selective absorber coating of WAlN/WAlON/Al_2O_3 for solar thermal applications, Solar Energy Materials and Solar Cells, 157 (2016) 716-726.
[16] A. Dan, K. Chattopadhyay, H.C. Barshilia, B. Basu, Thermal stability of WAlN/WAlON/Al_2O_3-based solar selective absorber coating, MRS Advances, (2016) 1-7.
[17] A. Dan, K. Chattopadhyay, H.C. Barshilia, B. Basu, Angular solar absorptance and thermal stability of W/WAlN/WAlON/Al_2O_3-based solar selective absorber coating, Applied Thermal Engineering, 109 (2016) 997-1002.
[18] J. De Feijter, d.J. Benjamins, F.A. Veer, Ellipsometry as a tool to study the adsorption behavior of synthetic and biopolymers at the air–water interface, Biopolymers, 17 (1978) 1759-1772.
[19] G.E. Jellison Jr, Spectroscopic ellipsometry data analysis: measured versus calculated quantities, Thin solid films, 313 (1998) 33-39.
[20] G.E. Jellison, V.I. Merkulov, A.A. Puretzky, D.B. Geohegan, G. Eres, D.H. Lowndes, J.B. Caughman, Characterization of thin-film amorphous semiconductors using spectroscopic ellipsometry, Thin Solid Films, 377 (2000) 68-73.
[21] G.E. Jellison Jr, F.A. Modine, Parameterization of the optical functions of amorphous materials in the interband region, Applied Physics Letters, 69 (1996) 371-373.
[22] G.E. Jellison Jr, F.A. Modine, P. Doshi, A. Rohatgi, Spectroscopic ellipsometry characterization of thin-film silicon nitride, Thin Solid Films, 313 (1998) 193-197.
[23] G. Ghosh, Handbook of optical constants of solids: Handbook of thermo-optic coefficients of optical materials with applications, Academic Press, 1998.
[24] D. Bhattacharyya, A. Biswas, Spectroscopic ellipsometric study on dispersion of optical constants of Gd 2 O 3 films, Journal of applied physics, 97 (2005) 053501.
[25] B. von Blanckenhagen, D. Tonova, J. Ullmann, Application of the Tauc-Lorentz formulation to the interband absorption of optical coating materials, Applied optics, 41 (2002) 3137-3141.

[26] J. Orava, J. Šik, T. Wagner, M. Frumar, Optical properties of $As_{33}S_{67-x}Se_x$ bulk glasses studied by spectroscopic ellipsometry, Journal of Applied Physics, 103 (2008) 083512.
[27] Z. Wang, X. Cai, Q. Chen, L. Li, Optical properties of metal-dielectric multilayers in the near UV region, Vacuum, 80 (2006) 438-443.
[28] M.A. Ordal, L.L. Long, R.J. Bell, S.E. Bell, R.R. Bell, R.W. Alexander, C.A. Ward, Optical properties of the metals al, co, cu, au, fe, pb, ni, pd, pt, ag, ti, and w in the infrared and far infrared, Applied Optics, 22 (1983) 1099-1119.
[29] M.A. Ordal, R.J. Bell, R.W. Alexander, L.L. Long, M.R. Querry, Optical properties of fourteen metals in the infrared and far infrared: Al, Co, Cu, Au, Fe, Pb, Mo, Ni, Pd, Pt, Ag, Ti, V, and W, Applied optics, 24 (1985) 4493-4499.
[30] V.D.A.G. Bruggeman, Berechnung verschiedener physikalischer Konstanten von heterogenen Substanzen. I. Dielektrizitätskonstanten und Leitfähigkeiten der Mischkörper aus isotropen Substanzen, Annalen der physik, 416 (1935) 636-664.
[31] H. Bartzsch, S. Lange, P. Frach, K. Goedicke, Graded refractive index layer systems for antireflective coatings and rugate filters deposited by reactive pulse magnetron sputtering, Surface and Coatings Technology, 180 (2004) 616-620.
[32] J. Borges, N.P. Barradas, E. Alves, M.F. Beaufort, D. Eyidi, F. Vaz, L. Marques, Influence of stoichiometry and structure on the optical properties of AlN_xO_y films, Journal of Physics D: Applied Physics, 46 (2012) 015305.
[33] G. Soto, W. De la Cruz, F.F. Castillon, J.A. Dıaz, R. Machorro, M.H. Farıas, Tungsten nitride films grown via pulsed laser deposition studied in situ by electron spectroscopies, Applied surface science, 214 (2003) 58-67.
[34] J.S. Becker, S. Suh, S. Wang, R.G. Gordon, Highly conformal thin films of tungsten nitride prepared by atomic layer deposition from a novel precursor, Chemistry of materials, 15 (2003) 2969-2976.
[35] S.H. Mohamed, A. Anders, Structural, optical and electrical properties of WO_xN_y films deposited by reactive dual.
[36] P. Pérez-Romo, C. Potvin, J.M. Manoli, G. Djéga-Mariadassou, Phosphorus-doped tungsten oxynitrides: Synthesis, characterization, and catalytic behavior in propene hydrogenation and n-heptane isomerization, Journal of Catalysis, 205 (2002) 191-198.
[37] G. Huff, E. Squitieri, P.E. Snyder, The heat of formation of tungstic oxide, WO_3, J Am Chem Soc, 70 (1948) 3380.
[38] T.V. Charlu, O.J. Kleppa, High-temperature combustion calorimetry 1. Enthalpies of formation of tungsten oxides, The Journal of Chemical Thermodynamics, 5 (1973) 325-330.
[39] M. Uekubo, T. Oku, K. Nii, M. Murakami, K. Takahiro, S. Yamaguchi, T. Nakano, T. Ohta, WN x diffusion barriers between Si and Cu, Thin Solid Films, 286 (1996) 170-175.
[40] F.R. De Boer, W.C.M. Mattens, R. Boom, A.R. Miedema, A.K. Niessen, Cohesion in metals, (1988).
[41] M.A. Frisch, J.L. Margrave, The Heat of Formation of Nitric Oxide(g), The Journal of Physical Chemistry, 69 (1965) 3863-3866.
[42] M. Gillet, C. Lemire, E. Gillet, K. Aguir, The role of surface oxygen vacancies upon WO_3 conductivity, Surface Science, 532 (2003) 519-525.
[43] A.H.Y. Hendi, M.F. Al-Kuhaili, S.M.A. Durrani, M.M. Faiz, A. Ul-Hamid, A. Qurashi, I. Khan, Modulation of the band gap of tungsten oxide thin films through mixing with cadmium telluride towards photovoltaic applications, Materials Research Bulletin, 87 (2017) 148-154.
[44] J. Li, M. Yahiro, K. Ishida, H. Yamada, K. Matsushige, Enhanced performance of organic light emitting device by insertion of conducting/insulating WO_3 anodic buffer layer, Synthetic Metals, 151 (2005) 141-146.
[45] E.O. Filatova, A.S. Konashuk, Interpretation of the changing the band gap of Al_2O_3 depending on its crystalline form: connection with different local symmetries, The Journal of Physical Chemistry C, 119 (2015) 20755-20761.

[46] J.K. Kim, A.N. Noemaun, F.W. Mont, D. Meyaard, E.F. Schubert, D.J. Poxson, H. Kim, C. Sone, Y. Park, Elimination of total internal reflection in GaInN light-emitting diodes by graded-refractive-index micropillars, Applied Physics Letters, 93 (2008) 221111.
[47] A. Dan, K. Chattopadhyay, H.C. Barshilia, B. Basu, Colored selective absorber coating with excellent durability, Thin Solid Films, 620 (2016) 17-22.

Table

Table 1: Best fit ellipsometric parameters of TL dispersion model for WAlN and Al_2O_3 single layer coating on SS substrate

Coating	Parameters of TL dispersion model				
	E_g (eV)	ε_∞	A	E_0 (eV)	C
WAlN	0.036	0.278	358.01	21.57	233.39
Al_2O_3	6.71	1.15	99.44	11.15	0.26

Table 2: Best fit ellipsometric parameters of Cauchy absorbent model for WAlON single layer coating on SS substrate

Coating	Parameters of Cauchy absorbent model					
	A	B	C	D	E	F
WAlON	1.86	1.64	1.59	1146.34	-0.40	0.830

Table 3: The optical constants (n and k at 550 nm) of all the layers

Layer	Optical constants at 550 nm	
	Refractive index (n)	Extinction coefficient (k)
WAlN	2.971	1.299
WAlN-WAlON	2.188	0.255
WAlON	1.940	0.007
WAlON-Al_2O_3	1.806	0.004
Al_2O_3	1.614	0

Figure

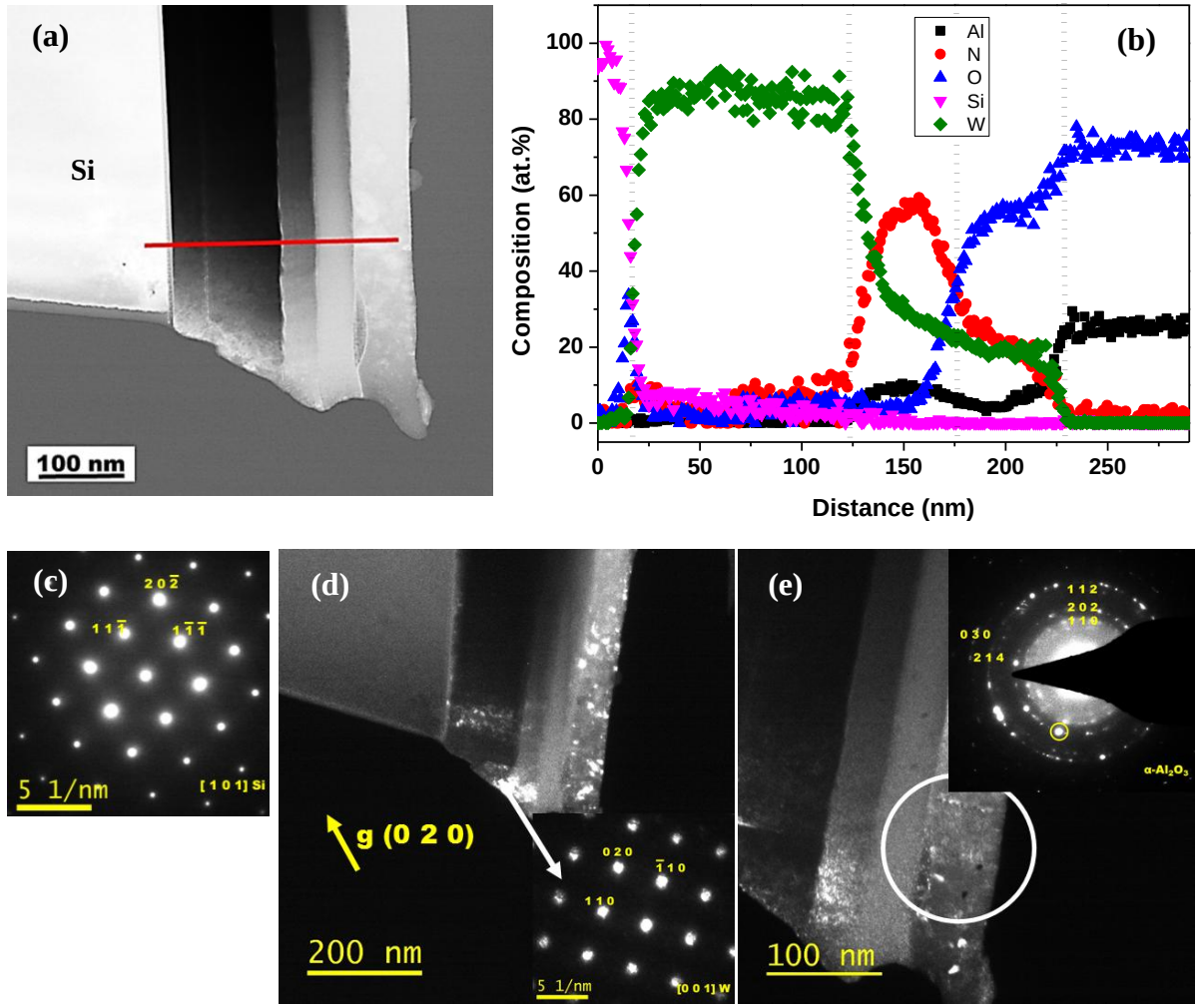

Fig. 1. (a) STEM dark-field image (cross-sectional view) of W/WAlN/WAlON/Al_2O_3 thin layers deposited on single crystal Si substrate, (b) concentration profiles of elements present in all four layers acquired using STEM-EDS detector from a region marked in the image with the red color line. (c) SAD pattern acquired from the substrate indexed in terms of [101] zone axis of Si, (d) dark-field showing the illuminated crystalline grains present in W layer and very fine nanograins in WAlN and Al_2O_3 layers and a SAD pattern acquired from a region marked by white arrow which can be indexed in terms of [001] zone axis of bcc W. (e) dark-field image with a SAD pattern as inset acquired from a region marked by white circle and spotty rings can be indexed with the reflection of hexagonal α-Al_2O_3.

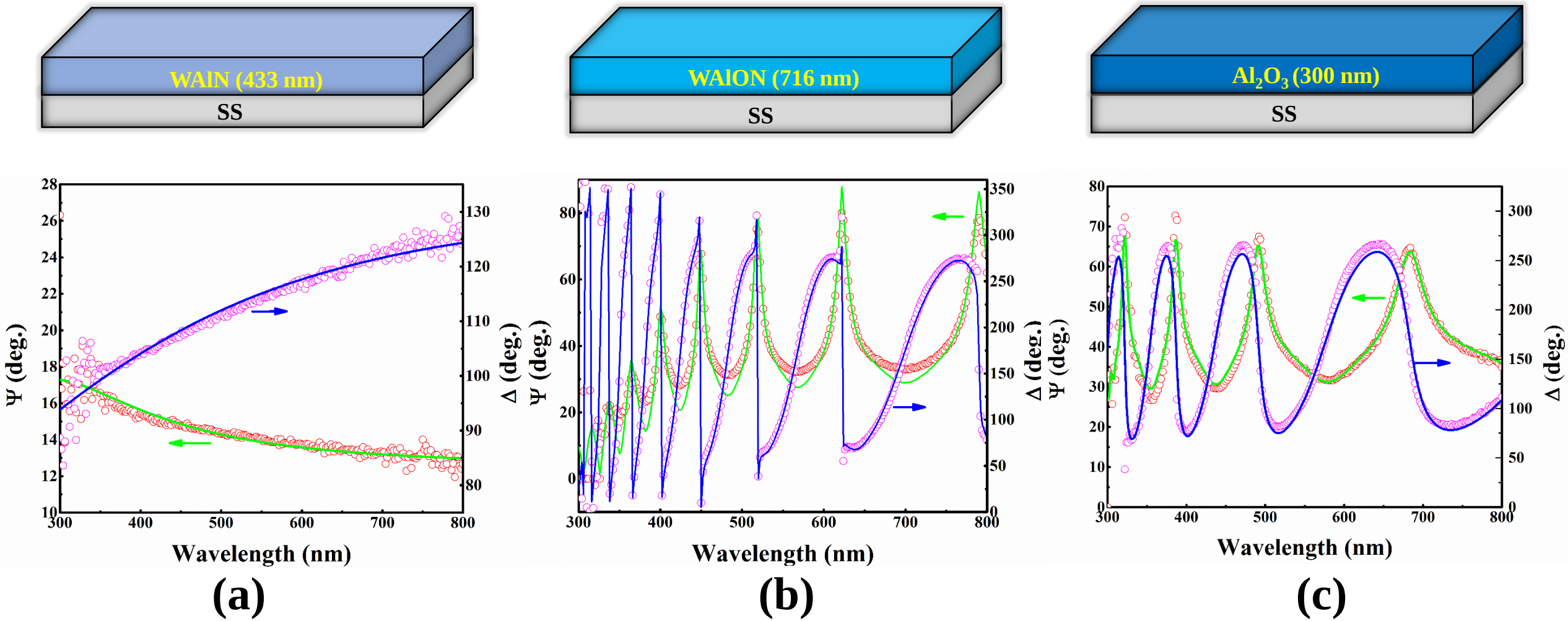

Fig. 2. Phase modulated ellipsometry spectra for (a) WAlN, (b) WAlON, and (c) Al_2O_3 single layer thin film on SS substrates deposited for prolonged duration, along with their respective models shown in the schematics above the graphs. The open symbols (o) represent experimental data, while the solid lines (-) are obtained from the fitting procedure. Thickness of individual layer is also mentioned.

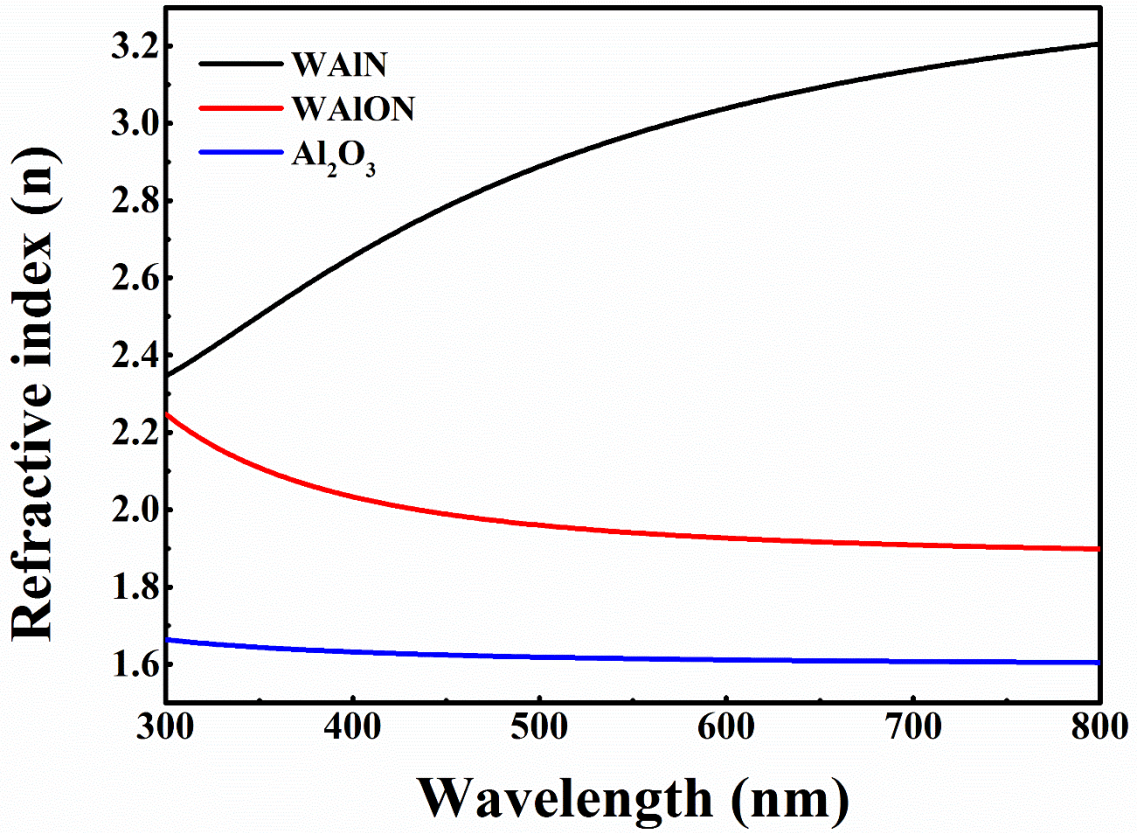

(a)

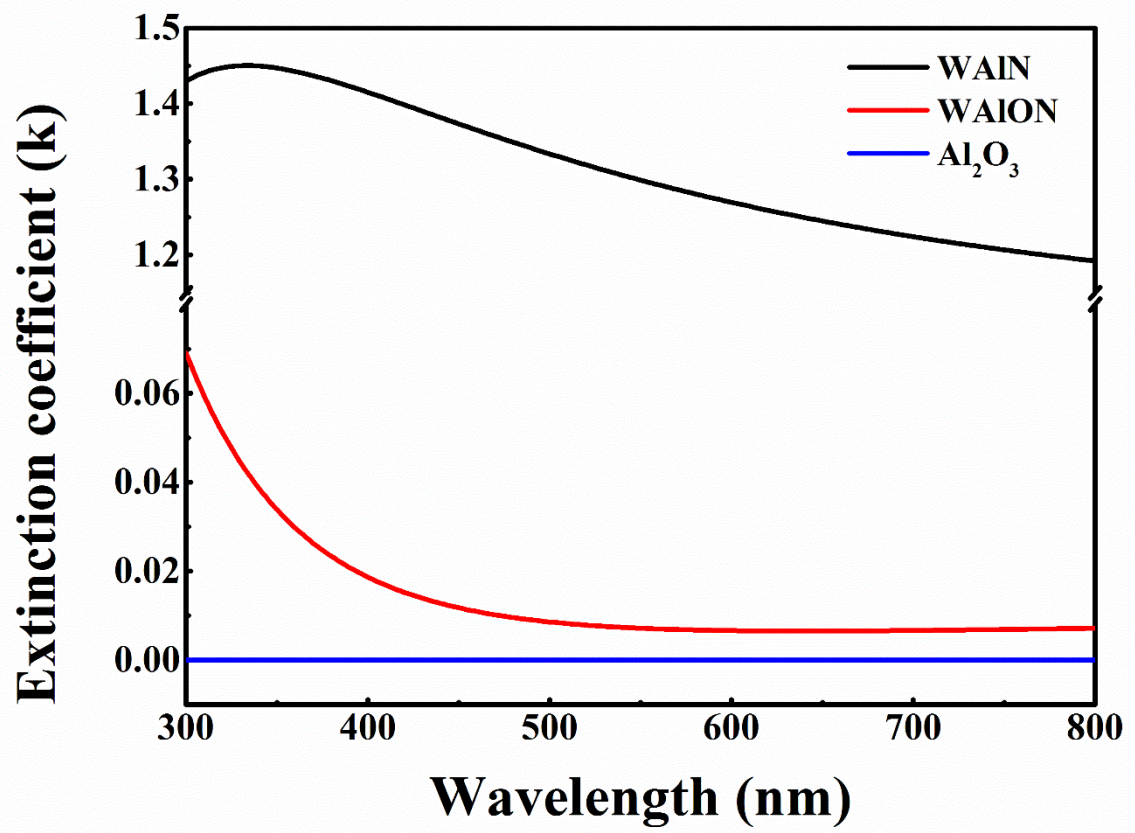

(b)

Fig. 3. Variation of (a) refractive index and (b) extinction coefficient with wavelength for WAlN, WAlON and Al_2O_3 single layer coatings on SS substrates, as shown in Fig. 2.

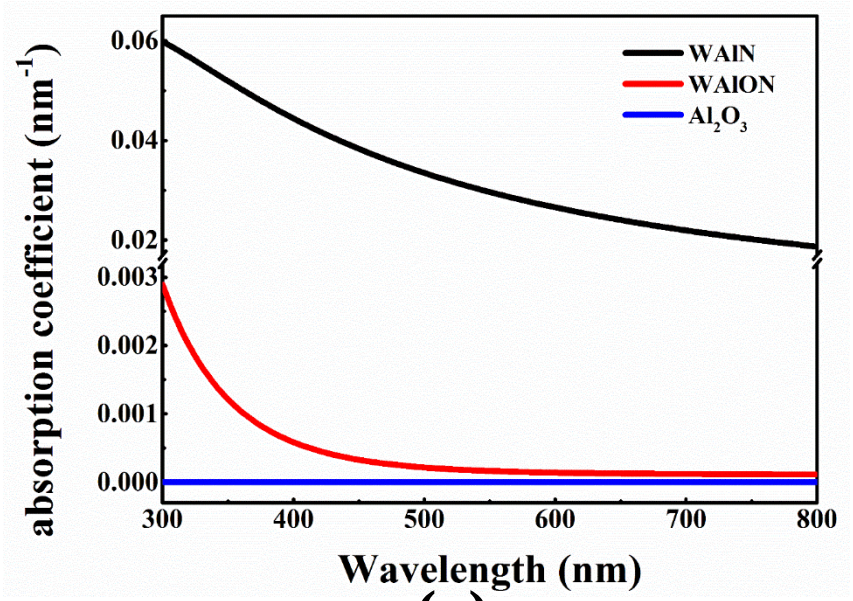

(a)

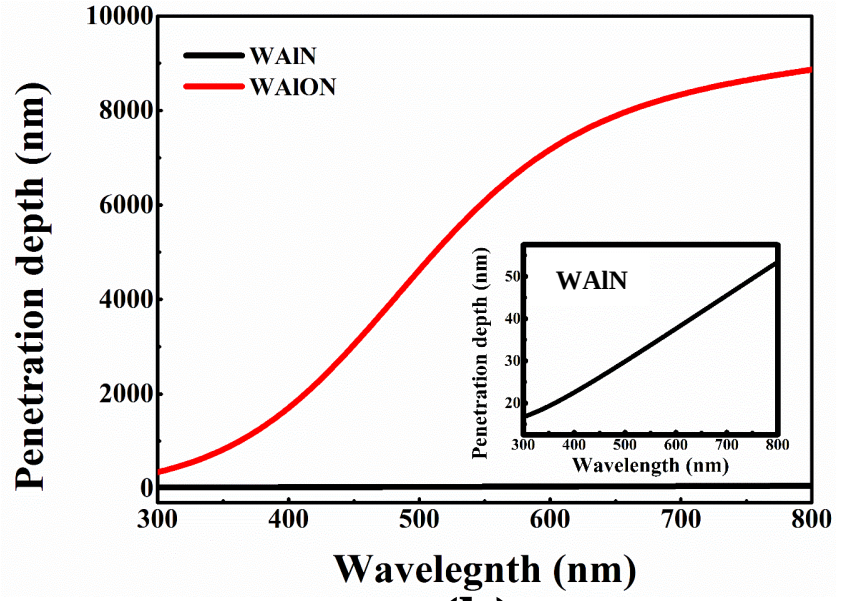

(b)

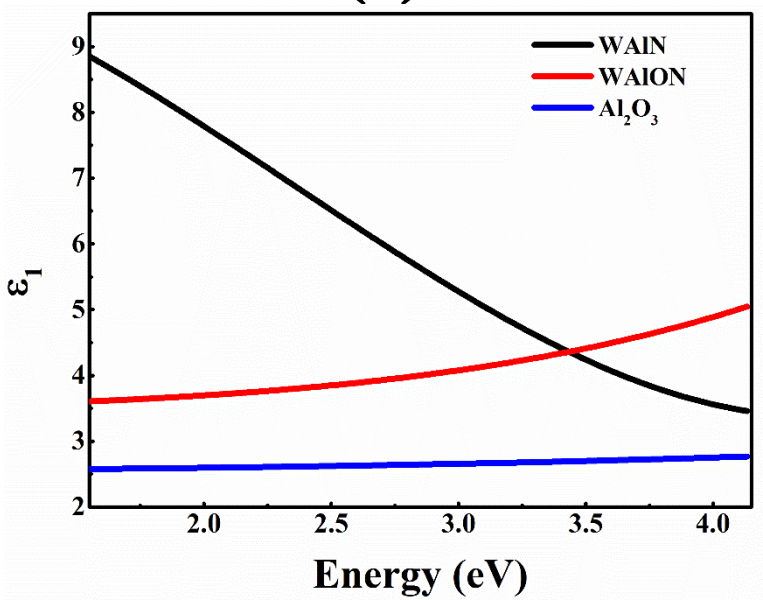

(c)

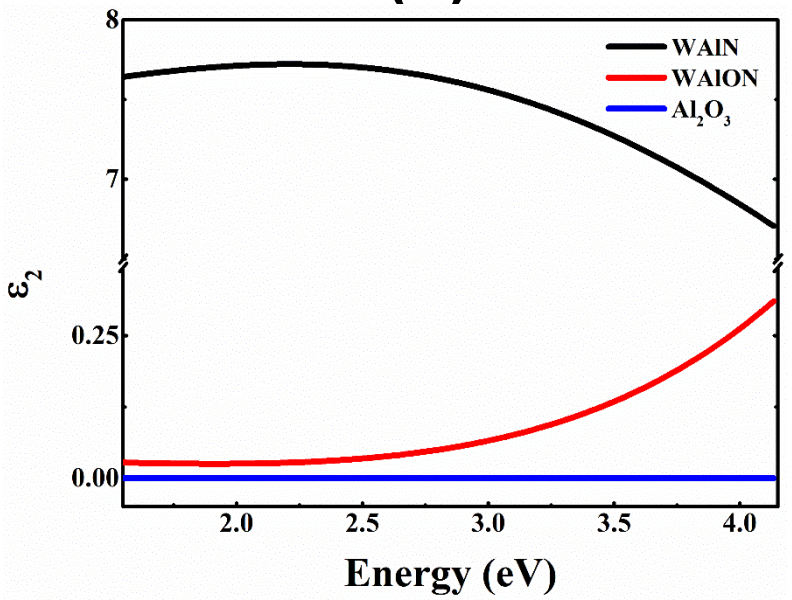

(d)

Fig. 4. (a) Absorption coefficient, (b) penetration depth (The inset shows the penetration depth of WAlN separately), (c) real (ε_1), and (d) imaginary (ε_2) part of the dielectric constants as function of wavelength for single layer coatings deposited on SS substrates, as shown in Fig. 2.

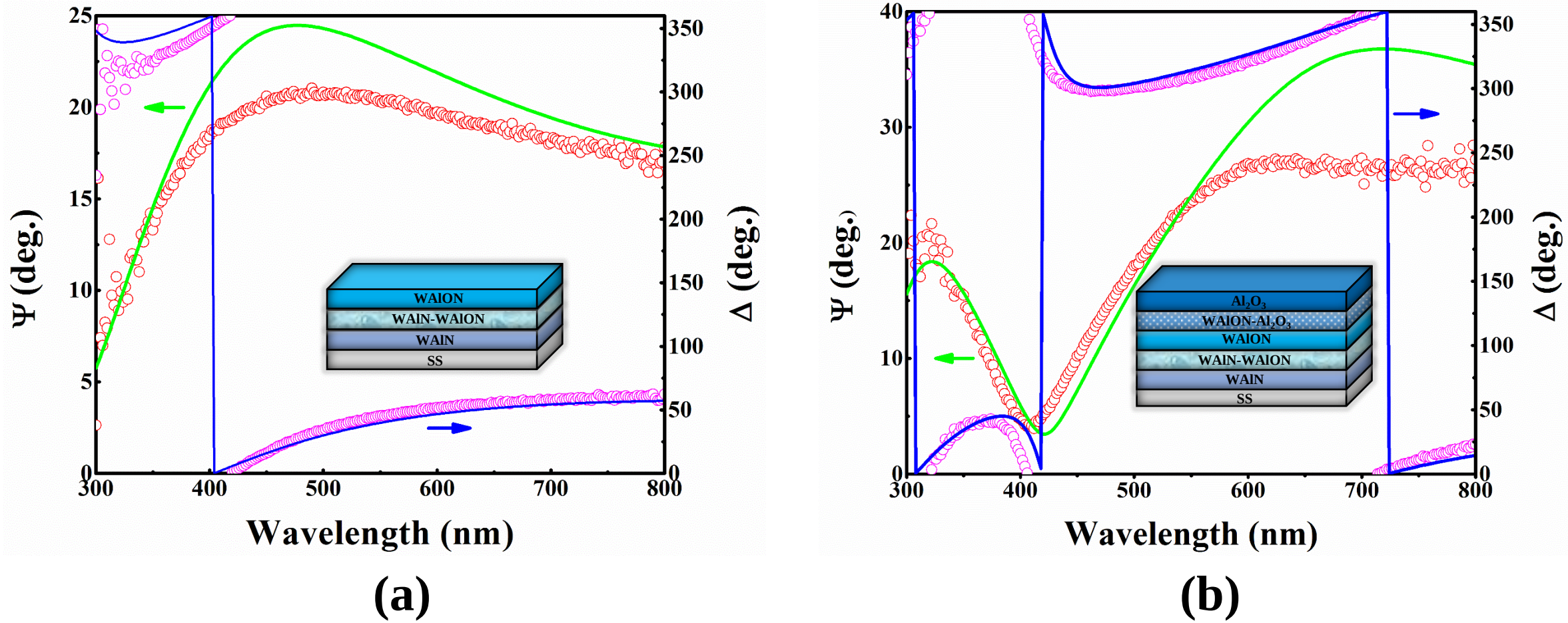

Fig. 5. Experimental (symbols) and fitted (solid lines) ellipsometric data for (a) WAlN/WAlN-WAlON/WAlON and (b) WAlN/WAlN-WAlON/WAlON/WAlON-Al_2O_3/Al_2O_3 layers on SS substrate; Insets show schematic representation of proposed structures used to perform the fitting.

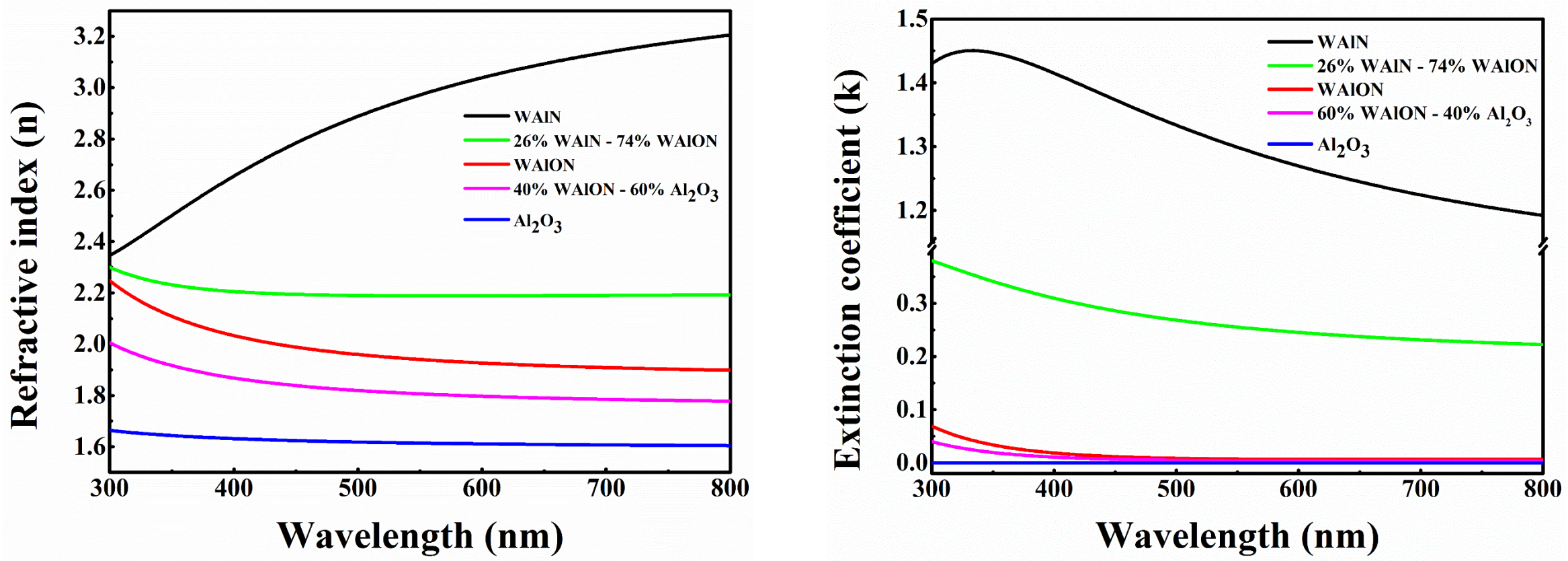

Fig. 6. (a) Refractive index (n) and (b) extinction coefficient of individual layer of multilayer stack (see inset in Fig. 5(b)).

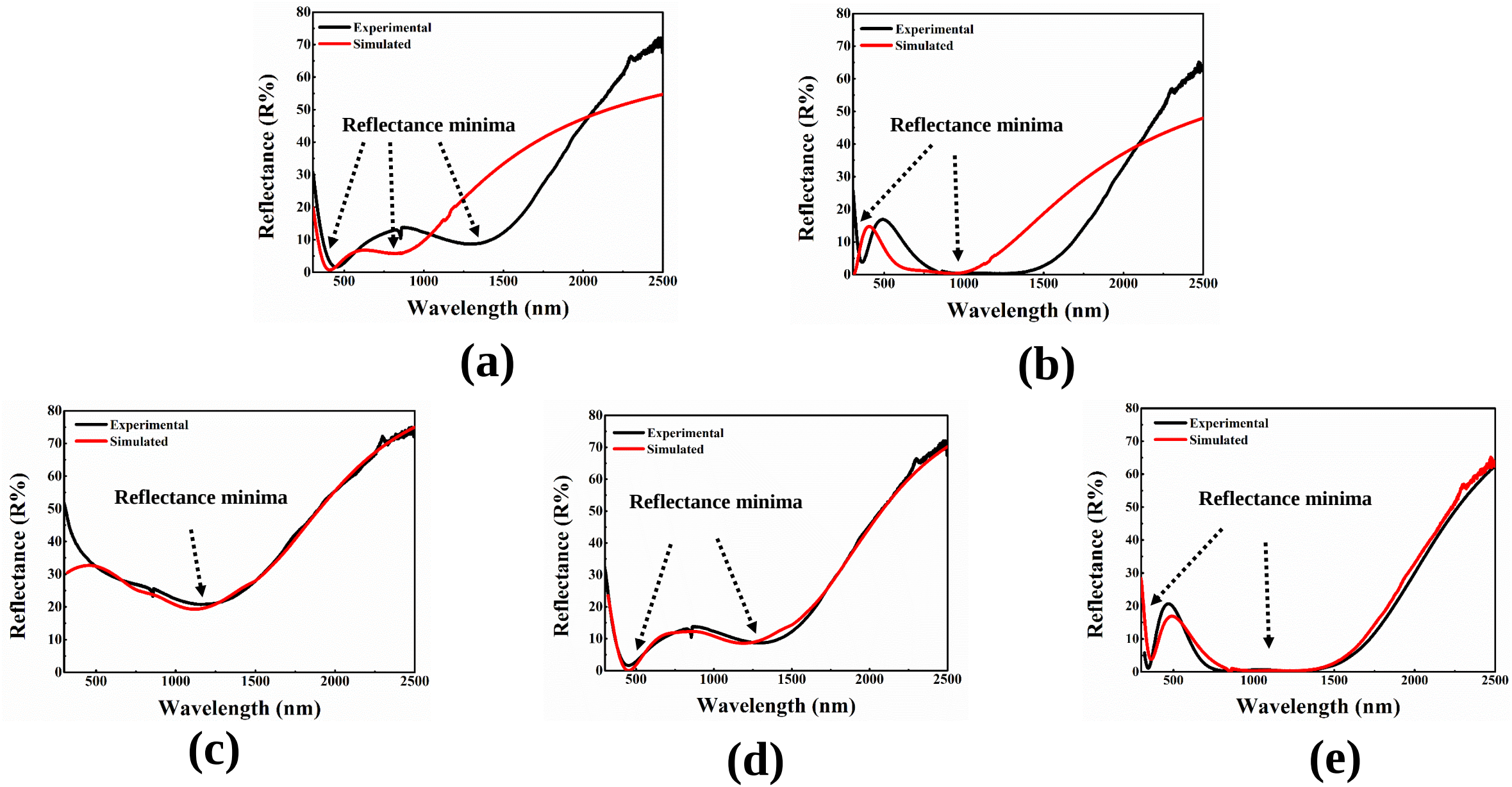

Fig. 7. Experimental (black) and simulated (red) reflectance spectra of (a) SS/WAlN/WAlON, (b) SS/WAlN/WAlON/Al_2O_3, (c) SS/WAlN, (d) SS/WAlN/WAlN-WAlON/WAlON, and (e) SS/WAlN/WAlN-WAlON/WAlON/WAlON-Al_2O_3/Al_2O_3 coatings in solar wavelength range.